

PAPER • OPEN ACCESS

# Unconventional long range triplet proximity effect in planar $\text{YBa}_2\text{Cu}_3\text{O}_7/\text{La}_{0.7}\text{Sr}_{0.3}\text{MnO}_3/\text{YBa}_2\text{Cu}_3\text{O}_7$ Josephson junctions







To cite this article: David Sanchez-Manzano *et al* 2023 *Supercond. Sci. Technol.* **36** 074002

View the [article online](#) for updates and enhancements.

You may also like

- [Strong-coupling topological Josephson effect in quantum wires](#)  
Flavio S Nogueira and Ilya Eremin
- [Magnetoelectric effects in Josephson junctions](#)  
I V Bobkova, A M Bobkov and M A Silaev
- [Anomalous Josephson effect](#)  
Yu M Shukrinov

# Unconventional long range triplet proximity effect in planar $\text{YBa}_2\text{Cu}_3\text{O}_7/\text{La}_{0.7}\text{Sr}_{0.3}\text{MnO}_3/\text{YBa}_2\text{Cu}_3\text{O}_7$ Josephson junctions

David Sanchez-Manzano<sup>1</sup> , S Mesoraca<sup>1</sup>, F Cuellar<sup>2</sup>, M Cabero<sup>3,4</sup>, S Rodriguez-Corvillo<sup>2</sup>, V Rouco<sup>2</sup>, F Mompean<sup>5,6</sup>, M Garcia-Hernandez<sup>5,6</sup> , J M Gonzalez-Calbet<sup>4,7</sup>, C Feuillet-Palma<sup>8</sup> , N Bergeal<sup>8</sup>, J Lesueur<sup>8</sup> , C Leon<sup>2</sup> , Javier E Villegas<sup>1</sup> and J Santamaria<sup>2,6,\*</sup> 

<sup>1</sup> Unité Mixte de Physique, CNRS, Thales, Université Paris-Saclay, 91767 Palaiseau, France

<sup>2</sup> GFMC. Department Física de Materiales. Facultad de Física. Universidad Complutense, Madrid 28040, Spain

<sup>3</sup> IMDEA Nanoscience Campus Universidad Autonoma, 28049 Cantoblanco, Spain

<sup>4</sup> Centro Nacional de Microscopia Electronica. Universidad Complutense, Madrid 28040, Spain

<sup>5</sup> Instituto de Ciencia de Materiales de Madrid ICMM-CSIC, 28049 Cantoblanco, Spain

<sup>6</sup> Unidad Asociada UCM/CSIC, 'Laboratorio de Heteroestructuras con aplicación en spintrónica', Cantoblanco 28049, Spain

<sup>7</sup> Department Química Inorganica. Facultad de Química. Universidad Complutense, Madrid 28040, Spain

<sup>8</sup> Laboratoire de Physique et d'Etude des Matériaux, CNRS, ESPCI Paris, PSL Research University, UPMC, 75005 Paris, France

E-mail: [jacsan@ucm.es](mailto:jacsan@ucm.es)

Received 1 January 2023, revised 13 March 2023

Accepted for publication 6 April 2023

Published 5 June 2023



CrossMark

## Abstract

The proximity effect between superconductors and ferromagnets may become long range due to the generation of triplet pairs. The recent finding of a long, one micron-range unconventional Josephson effect between  $\text{YBa}_2\text{Cu}_3\text{O}_7$  high Tc cuprates separated by a half metallic  $\text{La}_{0.7}\text{Sr}_{0.3}\text{MnO}_3$  manganite ferromagnet has uncovered a novel unconventional triplet proximity effect. In this paper, we examine the temperature dependence of the critical current in planar Josephson junctions. We find that the critical current—normal resistance product follows the predictions of traditional superconductor-normal metal-superconductor junctions, which implies that triplet pairs in a ferromagnet are transported in the diffusive limit similarly to singlet pairs in a normal metal. This result calls for theoretical studies of the new triplet Josephson effect and underlines its potential in future superconducting spintronics.

Keywords: proximity effect, unconventional superconductivity, Josephson effect

(Some figures may appear in colour only in the online journal)

\* Author to whom any correspondence should be addressed.



Original content from this work may be used under the terms of the [Creative Commons Attribution 4.0 licence](https://creativecommons.org/licenses/by/4.0/). Any further distribution of this work must maintain attribution to the author(s) and the title of the work, journal citation and DOI.

## 1. Introduction

The traditional antagonism between ferromagnetism and superconductivity had to be reconsidered in the early 2000s when seminal theoretical papers showed the possibility of triplet Cooper pairs being generated at ferromagnet/superconductor (F/S) interfaces [1–9]. Soon after, extensive experimental evidence appeared of long range supercurrents in F's in contact with S's, supporting the existence of a long range triplet F/S proximity effect [10–13]. At the microscopic level, triplet generation results from spin mixing and spin rotation processes driven by magnetic inhomogeneities and spin flip scattering [5, 7, 8, 10–15]. Long range supercurrents have been observed in vertical and lateral F/S structures in several material scenarios fueling the dream of superconducting spintronics [16, 17].

Despite many hints of triplet superconductivity producing long range supercurrents, very long range Josephson effects have remained elusive, especially in the case of unconventional high-temperature S's combined with half-metallic F's [18–23]. A major breakthrough is the recent finding of a long micron-range unconventional Josephson effect across a half metal [24]. Planar Josephson junctions where superconducting cuprate  $\text{YBa}_2\text{Cu}_3\text{O}_7$  (YBCO) electrodes are coupled across half-metallic manganite  $\text{La}_{0.7}\text{Sr}_{0.3}\text{MnO}_3$  (LSMO) wire show in addition to large critical currents, the hallmarks of Josephson effect: (i) critical current oscillations under applied magnetic fields driven by magnetic flux quantization (Fraunhofer pattern); and (ii) quantum phase locking effects under microwave excitation (Shapiro steps). Being YBCO an unconventional d-wave S, this study has raised important questions regarding the origin of the triplet proximity effect, and what is the symmetry of the pairing amplitude driving the long range Josephson coupling. In this paper, we aim at exploring the proximity effect in the YBCO/LSMO/YBCO system from an analysis of the temperature dependence of the critical current in planar Josephson junctions with different lengths of the LSMO weak link.

The presence of supercurrent and Josephson effects in S-normal metal (N)- Superconductor structures (SNS) has its origin in the proximity effect [25], by which superconducting correlations in the N are mediated by Andreev pairs generated by phase coherent Andreev reflections at the S-N interfaces. The coherence length in the N  $\xi_N$  takes the form  $\xi_N = (\frac{\hbar D}{2\pi k_B T})^{1/2}$  (where D is the diffusion coefficient) which can take long (micron-size) values at low temperatures. If the N is an F the superconducting correlations decay fast as phase coherence between Andreev pairs is broken by the exchange field. i.e. the correlation length in the F  $\xi_{FM}$  takes the form  $\xi_{FM} = (\frac{\hbar D}{h_{ex}})^{1/2}$  (where  $h_{ex}$  is the exchange field, namely the exchange splitting between both spin bands due to the exchange interaction) [3, 4]. For homogeneous exchange fields  $\xi_{FM}$  is typically very short, a few nanometers in the case of weak F's with small values of the exchange field, and much shorter values are expected in the case of strong F with  $\sim 1$  eV range exchange splitting. The situation, however, changes under inhomogeneous exchange fields, if spin triplet pairs are generated [3, 4], since they would not be affected by the exchange field. Moreover, in

the case (like ours) of half metals where the conduction band is fully spin polarized, the (femto-second) spin flip route characteristic of metals, the Elliott Yafet mechanism, caused by spin-orbit driven spin mixing at high symmetry points, is blocked resulting from the vanishing minority spin density of states at the Fermi level. As a result, there is no spin channel for spin-flip scattering and the energy has to be transferred through the less efficient spin-lattice relaxation with a longer time scale ( $\tau_{SF} \sim 200\text{--}400$  ps) as discussed in [26]. In the half metal/S proximity scenario, as a result of the blocked spin-flip scattering channel, only thermal de-phasing of the Andreev pairs can occur.

In this sense, a half metallic weak link where the pairing amplitude is carried by triplet correlations should behave akin to a N one and follow the predictions of SNS theories for singlet pairs de-phasing only thermally. This is precisely the aim of this paper, we want to examine the temperature dependence of the critical current in planar junction devices to assess if triplets in a ferromagnetic weak link follow the predictions of the theory for conventional SNS junctions, which we briefly describe immediately below.

The critical current of an SNS junction is limited exponentially by the length  $L$  of the N weak link:  $I_c \propto e^{-\frac{L}{\xi_N}}$ . The theory of the critical current of SNS junctions in the diffusive limit was initially developed by Likharev [27, 28] using Usadel [29] equations. This is a high temperature approach valid close to the critical temperature where the thermal energy is larger than the superconducting gap. The extension to low temperatures, where experimental data have shown significant departures from early theories by de Gennes [25], was completed by Dubos and collaborators [30] using quasi-classical Green's functions.

Diffusive transport in junctions with an N weak link longer than the electron mean free path but shorter than the de-phasing length limits electron-hole coherence to an energy window given by the Thouless energy [31]  $E_{Th} = \frac{\hbar D}{L^2}$  (which should be smaller than the width of the thermal distribution). It is important to note that the Thouless energy is a single electron energy scale set by the diffusion rate of normal electrons across the sample. The low temperature calculation  $k_B T < E_{Th}$  by Dubos *et al* [30] involving the solution of Usadel equations at all energies provides, in the long junction limit ( $\frac{\Delta}{E_{Th}} \gg 1$ , with  $\Delta$  the superconducting gap), a simple analytic expression for the normal resistance-critical current  $eI_c R_n$  product, which reads:

$$eI_c R_n = \frac{32}{3 + 2\sqrt{2}} E_{Th} \left[ \frac{L}{\xi_N} \right]^3 e^{-\frac{L}{\xi_N}}. \quad (1)$$

With a zero temperature limit, which cuts-off the divergence of the critical current at low temperature of the early theories. It is worth to remark that at high temperatures where the thermal energy scale is larger than the gap ( $\frac{k_B T}{\Delta} \gg 1$ ) the full calculation recovers the result predicted by Likharev [28].

In discussing the superconducting properties of all oxide planar junction devices, an interesting connection is the so called 'long range proximity effect' observed in planar HTSC junctions with oxide semiconductor barriers showing long

range supercurrents for spacer layer thicknesses in excess of 100 nm [32–34]. Theoretical analysis [35–37] has shown that the long range transport of the Josephson current is governed by resonant tunneling via the localized states in the barrier.

## 2. Results and discussion

The samples used in this study were planar Josephson junctions [24] based on LSMO and YBCO microwires 20–25  $\mu\text{m}$  wide grown epitaxially on (001) SrTiO<sub>3</sub>. LSMO was grown on (001)-oriented SrTiO<sub>3</sub> single crystals in a pure oxygen d.c. sputtering system at high pressure (3.2 mbar) and elevated temperature 900 °C. *In situ* annealing was done at 800 °C with 900 mbar O<sub>2</sub> pressure for 1 h. Electron beam lithography was performed in a Raith50 module mounted on a SEM Zeiss EVO50 to obtain LSMO microwires and to define amorphous alumina patterns. This is an important step, since the usual process resists do not withstand the high temperatures used to grow these oxides. Amorphous alumina was grown in a d.c. sputtering at  $7.3 \cdot 10^{-3}$  mbar atmosphere (Argon/Oxygen 2:1) at room temperature. YBCO was grown on top of LSMO and a-ALO template in a high O<sub>2</sub> pressure (3.4 mbar) d.c. sputtering system at 900 °C. *In situ* annealing was done at 800 °C with 900 mbar O<sub>2</sub> pressure for 1 h. The spacing between YBCO contacts was  $\sim 1 \mu\text{m}$ . Figure 1 shows an optical microscope image of a typical device. The *ex situ* fabrication strategy followed where LSMO wires were first patterned by optical lithography, and then amorphous alumina templates (mechanical masks) were engineered by electron beam lithography to define the YBCO electrodes that did not degrade the structure nor the chemistry of the interfaces as compared to vertical structures grown *in situ*. Figure 1(c) shows a scanning transmission electron microscopy (STEM) high-resolution image of the YBCO/LSMO interface. It appears to be atomically sharp and highly ordered as in *in-situ* samples, which indicates that the growth at 900 °C in a pure oxygen plasma has the effect of (re)conditioning the surface after exposure to atmosphere or processing. Figure 1(c) displays an atomic resolution electron energy loss spectroscopy (EELS) false color elemental map of the interface showing Ba M<sub>4,5</sub> (red), La M<sub>4,5</sub> (yellow) and Mn L<sub>2,3</sub> (blue). As in the *in-situ* samples, interface termination corresponds to BaO facing MnO<sub>2</sub> planes with missing CuO chains at the interface [38, 39] thus providing a direct Cu-O-Mn superexchange path across the interface which induces a magnetic state in the Visani *et al* [40]. Moreover, the difference in chemical potentials gives rise to charge (electrons) transfer from the YBCO to the LSMO which depresses the magnetization [38] as assessed by polarized neutron reflectometry. Thus, charge transfer (depressed Mn magnetism) and bond reconstruction (induced magnetism in the Cu at the interface) may be, together with the magnetic domain structure of the LSMO below the YBCO electrodes, sources of magnetic inhomogeneity which may play a role in triplet generation. The planar junctions were wired in a four-point contacts configuration (see sketch in figure 1(b)) for transport measurements. Resistance was measured by injecting current along the YBCO electrodes and measuring voltage between the ends

of the LSMO microwire. Figure 1(c) shows the temperature dependence of the resistance for three different devices. An S-like resistive transition can be seen with steps corresponding to the resistive transition of the different LSMO regions with different strength of the proximity interaction. The LSMO directly underneath the YBCO electrodes proximitizes first and then, gradually, the bare LSMO between the YBCO electrodes.

To obtain the critical current,  $I(V)$  curves were measured as a function of temperature (figure 2(a)) using the same four point contacts configuration.  $R(T)$ ,  $R(H)$  and  $I(V)$  were performed in a helium close cycle cryostat down to 15 K applying a maximum current of 800  $\mu\text{A}$  and magnetic field up to 4000 Oe while measuring the voltage. Current was injected along the YBCO leads and voltage was measured at the ends of the LSMO wire. Although Josephson junctions are in principle two terminal devices, this configuration was chosen mainly because Al wire bonding yields less noisy, more stable electrical contacts for LSMO than for YBCO, yet it provides a measurement without the influence of the interface resistance between LSMO and YBCO. Control experiments in the usual Josephson junction geometry with all four contacts on the YBCO wires (with interface resistance now included in series) showed very similar results pointing to a highly transparent interface, with indeed negligible contribution of interface resistance compared to the normal state resistance of the LSMO wire.

In our junctions, we obtain normal resistances  $R_n$  in the range of 1–5 ohms, consistent with the usual low temperature resistivity values of single LSMO wires in the range  $80 \mu\Omega \text{cm}$ – $200 \mu\Omega \text{cm}$ .  $I$ – $V$  curves are non-hysteretic indicating a negligible internal capacitance as expected from strongly overdamped intrinsically shunted devices.  $I$ – $V$  plots show considerable rounding and low current and voltage levels, as recently observed in other Josephson junctions with ferromagnetic barriers [41]. In the following, we describe the temperature dependence of the critical current in our planar Josephson devices. In fact, see figure 2(b), the actual values of the critical current are much lower than anticipated from the linear scale plots, and a rather restrictive voltage criterion ( $\sim$ hundred of nanovolts) had to be used to reach the non-linear critical current regime. The analysis of the low voltage regime (below a few  $\mu\text{V}$ ) allows us to estimate the critical current, which takes values in the range of  $10^2$ – $10^3 \text{ A cm}^{-2}$ , much lower than the typical ones (a few  $10^7 \text{ A cm}^{-2}$ ) found in YBCO wires in a similar temperature range. Fits of the low-voltage portion of  $I(V)$  curves to the Ivachenko—Zil’berman model [42], see figure 2(c)), showed that the critical current is limited by thermal fluctuations. Figure 2(c) shows the  $I$  $V$  curves measured at 18, 30, 35 and 40 K (the same as in figure 2(b)) together with fits to the (analytic) expressions of the Ivachenko—Zil’berman model [42] (black lines). It becomes clear from these fits that, although the low-current rounding can be explained by the effect of thermal fluctuations, the whole voltage range cannot be fitted by that model. In order to fit the complete  $I$  $V$  curves (yellow lines in figure 2(c)), a non-linear excess voltage has to be added in series that accounts for the contribution, unavoidable

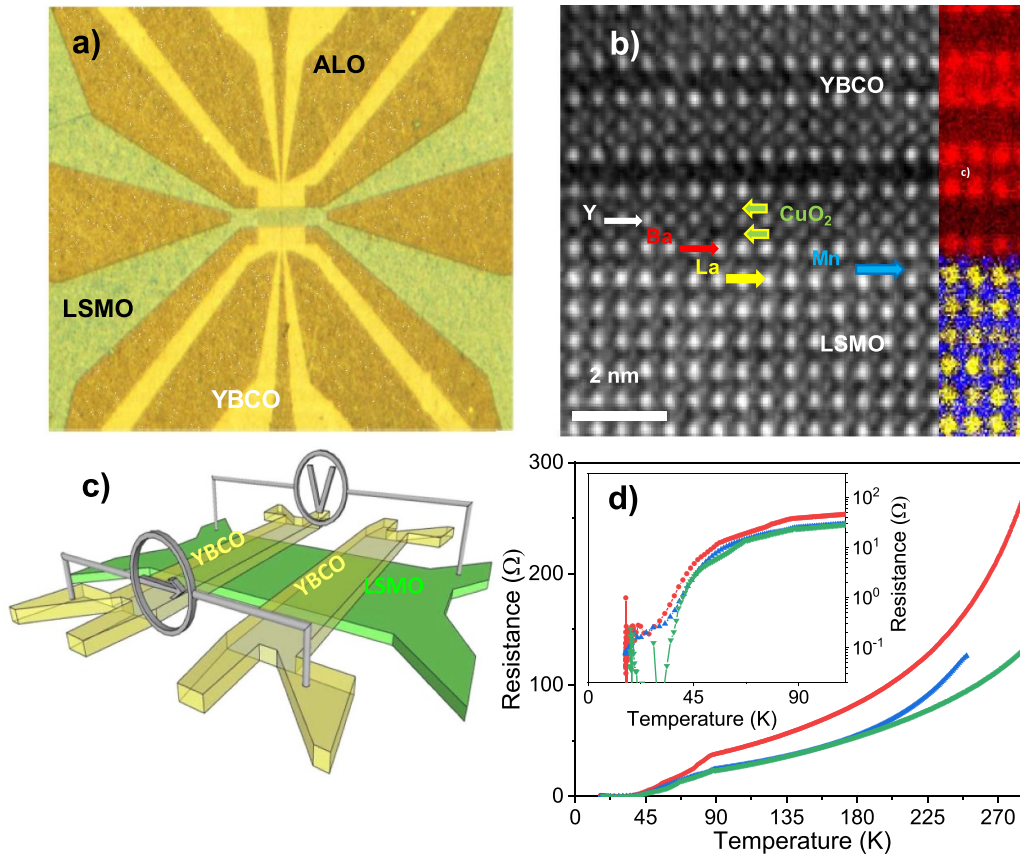


**Figure 1.** Structure and transport of planar YBCO/LSMO/YBCO devices. (a) Optical image of the device showing the amorphous  $\text{Al}_2\text{O}_3$  template to deposit YBCO. (b) Sketch showing the wiring of the devices to measure transport. (c) High resolution STEM-HAADF image of the same interface. Left: Atomic resolution HAADF image where atomic positions of each element are indicated by arrows in the different atomic columns. Right: Ba  $M_{4.5}$  (red), Mn  $L_{2.3}$  (blue) and La  $M_{4.5}$  (yellow) elemental EELS map in a color mix of a spectrum image of a region of interest from the same HAADF image. (d) Resistance vs. temperature of three different devices. Separation between YBCO contacts is  $1 \mu\text{m}$ . The width of the LSMO wire electrodes are  $20 \mu\text{m}$  (red)  $25 \mu\text{m}$  (blue and green). Reproduced from [24], with permission from Springer Nature.

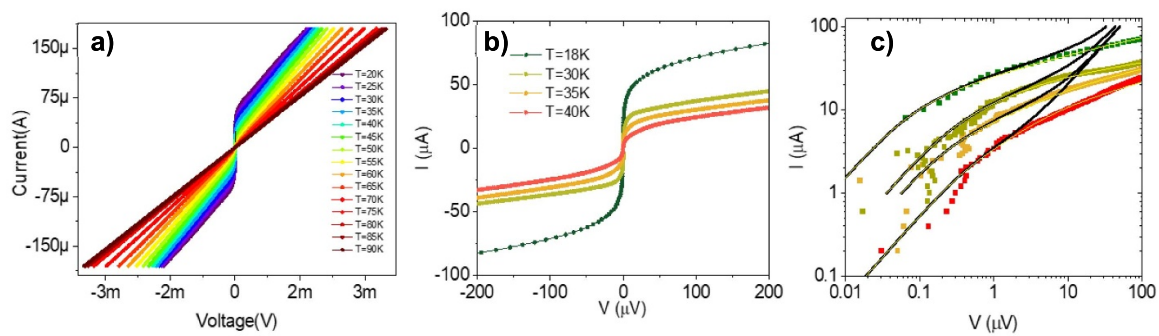


**Figure 2.** Temperature dependence of the critical current. (a)  $I$   $V$  curves as a function of temperature (left panel) (b)  $I$   $V$  curves at different temperatures between 18 K and 40 K. Panel adapted from [24] (c)  $I$   $V$  curves measured at 18, 30, 35 and 40 K from top to bottom in double logarithmic scale (symbols). The black lines are fits within the low current range, made according to the thermal rounding scenario described in [29]. These fits yield values of  $R_n = 0.5 \Omega$  at all temperatures and  $I_c = 60, 30, 15$  and  $5 \mu\text{A}$  (increasing temperature). Yellow lines result from adding to the black curves a nonlinear voltage term that accounts for contributions of the superconducting parts with higher critical current that are in series with the LSMO Josephson barrier. Reproduced from [24], with permission from Springer Nature.

is this type of planar Josephson devices [41], of other superconducting parts of the planar devices (YBCO electrodes and proximitized LSMO regions directly underneath the YBCO electrodes) which, despite their higher critical current, yield a

significant contribution to the device's resistance when a sufficiently high current is injected. The yellow lines in figure 2(c) have been obtained by adding a  $V \propto I^n$  term which is characteristic of YBCO in the critical current regime [43], with the

exponent  $n$  changing between 3 and 6 when the temperature is varied. The analysis, based on the Ivachenko—Zil'berman model [42], yields values of  $R_n = 0.5 \Omega$  at all temperatures and  $I_c = 60, 30, 15$  and  $5 \mu\text{A}$  (increasing temperature), which may be somewhat overestimated compared to the actual values. On the one hand, it validates independent estimates of the critical current and the junction's normal-state resistance  $R_n \sim 1 \text{ ohm}$  as obtained from this device (i) from the low-temperature resistivity of LSMO and (ii) from the resistance at the onset of resistive transition's last step. Notice that the normal state resistance cannot be obtained from a direct reading of the resistance at the critical temperature of the device due to the (dominant) series contribution of the resistance of other parts of the device. On the other hand, it provides an explanation for the substantial rounding of the  $I(V)$  curves and small critical current of the junctions in terms of thermal fluctuations, as one would indeed expect from the wide ferromagnetic barrier and the high critical temperature of the studied Josephson devices, showing that, in fact, thermal energy becomes comparable to Josephson energy ( $k_B T \sim \frac{\hbar I_c}{2e}$ ) at temperatures higher 40 K. Notice, finally that we cannot rule out that magnetic scattering of quasi particles may also contribute to the rounding of the  $I(V)$ , as suggested earlier [41], but in the present junctions this effect is probably weaker than that of thermal fluctuations given the high critical temperatures and the fact that the analysis based on thermal fluctuations provides by itself a close quantitative description of the data.

The finding of a long range supercurrent across a one micron long ferromagnetic barrier is a strong indication of triplet proximity, which was further confirmed [24] by flux matching effects of low temperature resistance and phase locking under microwave irradiation. We found a modulation of the resistance at the resistive transition by the (in plane) magnetic field at different angles with the [100] direction of the LSMO wire. Figure 3 shows the dependence of the resistance with the angle of the in plane magnetic field with the [100] (LSMO wire) direction measured  $T = 40 \text{ K}$ . Injected current was  $20 \mu\text{A}$ . This temperature is just below the onset of the resistive transition of the superconducting weak link. Notice that while at small magnetic fields (0.01 T) resistance is close to zero in the whole angular range, at larger fields (0.55 T) resistance is strongly modulated displaying sharp resistance peaks when the magnetic field is aligned with the [110] easy axes of the LSMO. Resistance is modulated by the variation of the (very small) critical current with magnetic field, and evidences its modulation with magnetization direction. This result, apart from proving the magnetic state of the weak link, strongly supports the triplet state of the pairing amplitude. Finally, we also found resistance modulation by out of plane magnetic field due to the Fraunhofer pattern modulation of the critical current by magnetic field (not shown) which is being analyzed and will be reported in the near future.

We have analyzed the scaling of the critical current with weak link length and temperature to verify that it follows the predictions of the theory of SNS junctions described above. We have prepared samples with different lengths of the LSMO weak link and looked at the temperature dependence of the critical current. Three different samples will be described here,

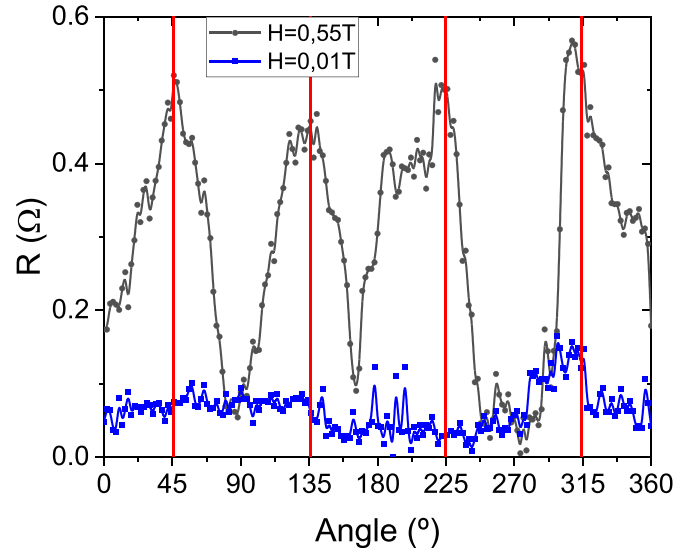


**Figure 3.** Magnetization dependence of the resistance. Angle dependence of the resistance at 0.01 T (blue symbols) and 0.55 T (black symbols) measured at  $25 \mu\text{A}$  and 40 K. Angle  $\theta$  refers to different orientations of the magnetic field with the [100] LSMO wire.

with weak link lengths 0.75, 1 and  $2 \mu\text{m}$ . The temperature dependence of the critical current of the sample with  $0.75 \mu\text{m}$  is displayed in figure 4(a). Notice the larger values of the critical current as compared to the  $1 \mu\text{m}$  sample shown in figure 4(b). This scaling is in accordance with the  $\frac{1}{L^2}$  size dependence of the Thouless energy. The  $2 \mu\text{m}$  showed no measurable critical current within our temperature window, which is also expected from the exponential suppression of the critical current (see below).

Notice that in the low temperature long junction approximation, the critical current features a temperature dependence of the form  $I_c \propto T^{3/2} e^{-\frac{T}{\xi_n}}$ . This dependence can be used to obtain directly the Thouless energy noting that the product  $I_c R_n$  in expression [1] can be written explicitly in terms of the Thouless energy as

$$e I_c R_n = \frac{32}{3 + 2\sqrt{2}} E_{\text{Th}} \left[ \frac{2\pi k_B T}{E_{\text{Th}}} \right]^{3/2} e^{-[2\pi k_B T / E_{\text{Th}}]^{1/2}}. \quad (2)$$

It follows, according to the analysis by Anwar *et al* [36, 37] that the critical current is proportional to  $T^{3/2} \exp\left(\sqrt{2\pi k_B T / E_{\text{Th}}}\right)$ . The linearity of  $\ln(I_c) - \frac{3}{2} \ln(T)$  vs  $\sqrt{T}$  is shown in figure 3(b) for the two superconducting samples. The slope provides a direct measure of the Thouless energy yielding  $95 \mu\text{eV}$  for the sample with  $1 \mu\text{m}$  LSMO weak link and  $150 \mu\text{eV}$  for the  $0.75 \mu\text{m}$  sample. These values, as we demonstrate below, are physically reasonable and compatible with previous analyses of the temperature dependence of SNS Josephson junctions, and in particular, with the analysis [12, 44] of the long range proximity effect in  $\text{CrO}_2$  (also a half metal) with low  $T_c$  S's.

The normal state resistance of the devices  $R_n$  was obtained from the lowest temperature step of the resistance curves and

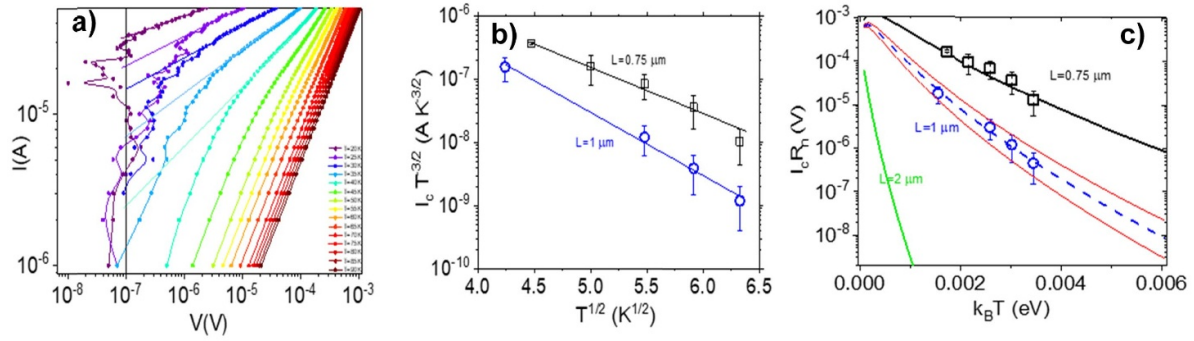


**Figure 4.** Analysis of the temperature dependence of the critical current. (a) Current–voltage ( $I$ – $V$ ) curves of a device with a smaller length of LSMO spacing of  $L = 0.75 \mu\text{m}$ . Lines connecting points are guides to the eye. (b) Analysis of the temperature dependence of the critical current to extract the Thouless energy (see main text). Notice the larger values of the critical current and the Thouless energy (smaller slope) of the  $0.75 \mu\text{m}$  long weak link (black symbols) compared with the  $L = 1 \mu\text{m}$  long weak link (blue symbols). (c)  $I_c R_n$  product for  $L = 2, 1$  and  $0.75 \mu\text{m}$ . Reproduced from [24], with permission from Springer Nature.

was found to be between 1 and  $2 \Omega$  for the  $1 \mu\text{m}$  sample, in agreement with the low temperature LSMO resistivity ( $80 \mu\Omega \text{cm}$ ) and bridge dimensions (width  $20 \mu\text{m} \times$  thickness  $30 \text{nm}$  for this device). This yields  $R_n$  values of the order of  $1.3 \Omega$ , which are consistent with the value estimated from the resistive transition. Following Dubos *et al* [30], further (rough) estimates can be gained from the current at a voltage value corresponding to the Thouless energy ( $95 \mu\text{eV}$ ) of the low temperature curves. The  $IV$  curve at  $18 \text{K}$  yields a value of  $1.3 \Omega$  in good agreement with our previous estimate. For the sample with  $0.75 \mu\text{m}$  LSMO spacer  $R_n$  was estimated to be  $5 \text{Ohm}$ , a value which, considering the device dimensions, is also consistent within the values of the resistivity and its range of variation for single LSMO wires. To assess whether samples with different spacer lengths scale according to the predictions of the SNS theory by Dubos *et al* [30], we constructed  $I_c R_n$  products with measured values of the critical current and the estimated  $R_n$  which follow the asymptotic expression in terms of the Thouless energy, equation (2). Figure 4(c) shows that experimental points closely follow the theoretical  $I_c R_n$  curve (equation (2)), for both samples. The open blue symbols correspond to the sample with LSMO spacing  $L = 1 \mu\text{m}$  and a Thouless energy of  $95 \mu\text{eV}$ . Red lines reflect the uncertainty in the determination of the Thouless energy according to error bars in the  $I_c R_n$  product:  $E_{\text{Th}} = 85 \mu\text{eV}$  (lower curve) and  $E_{\text{Th}} = 105 \mu\text{eV}$  (upper curve). The open black squares correspond to the sample with  $L = 0.75 \mu\text{m}$  and higher Thouless energy of  $150 \mu\text{eV}$ , as expected for the  $1/L^2$  scaling. Notice that for the sample with  $L = 2 \mu\text{m}$  no measurable critical current is expected in the accessible temperature range, as experimentally observed. This confirms that the critical current scales with device length as expected from the theory of SNS weak links, confirming that the measured critical current is physically reasonable in this theoretical framework. Furthermore, the fair agreement of the experimental long range triplet supercurrents to the predictions of the theory of (singlet pairs) SNS junctions indicates that triplet Andreev pairs diffuse in a half metallic F similar to how singlets do in an N.

A further important question concerns the symmetry of the triplet pairs in the orbital sector. The long range triplet

supercurrent has interesting implications on the symmetry of the pairing amplitude in the F [45]. Diffusive transport over micron long distances in the diffusive limit requires isotropic pairing to avoid de-phasing by random scattering events. This implies that the anisotropic d-wave pairing symmetry of the YBCO, established from Josephson interference experiments [46], would drastically suppress the critical current due to scattering induced de-phasing. Isotropic (s-wave) pairing is thus expected on general theoretical grounds [47]. In fact, it has been proposed that in junctions involving high  $T_c$  S's and F's with domain walls perpendicular to the interface [40], the generation of an odd-frequency triplet s-wave component of the condensate may give rise to long range penetration of the superconductivity in the F along the domain wall. On the other hand, strong on-site Coulomb repulsion present in all cuprates and manganites would, in principle, not favor simple s-wave pairing to avoid the strong repulsion at short range. An intriguing possibility is whether pairing may happen in some higher angular momentum channel in order to avoid the short-range repulsion. Pairing states with broken time-reversal symmetry, such as mixed ( $dx^2 - y^2 \pm is$ )- or ( $dx^2 - y^2 \pm idxy$ )-wave pairing states [48–50] are possible in the presence of broken spatial and temporal symmetries in our planar devices with ferromagnetic weak links. Moreover, for a cylindrical Fermi surface, this state is nodeless which optimizes the condensation energy and it avoids the [110] zero energy Andreev bound states (which suppress the d-wave order parameter upon scattering). Future experiments will be directed to address these exciting possibilities.

In summary, we have found that the critical current of planar Josephson junctions combining high  $T_c$  S's and half metallic manganites follows the predictions of the SNS theory for conventional proximity coupled Josephson junctions. This result suggests that fully spin polarized triplet Andreev pairs diffuse in the half metal similarly to singlets in an N. The very long (micrometric) distance over which phase coherent transport has been found underlines the potential of these devices in future superconducting spintronics. Furthermore, the possibility of controlling the spin polarized supercurrents with the

domain state of the F opens interesting opportunities for novel concepts of quantum switches and quantum memories.

### Data availability statement

Data will be available from the corresponding author upon reasonable request.

### Acknowledgments

Work supported by Spanish AEI through Grant PID2020-118078RB-I00 and by Regional Government of Madrid CAM through SINERGICO Project Y2020/NMT-6661 CAIRO-CM. Work at CNRS/Thales lab supported by ERC Grant No. 647100 ‘SUSPINTRONICS’, French ANR Grant ANR-15-CE24-0008-01 ‘SUPERTRONICS’ and COST action ‘Nanoco-hybrí’. We acknowledge funding from Flag ERA ERA-NET To2Dox Project. J E V thanks C Ulysse and L Vila for collaboration in related projects.

### Conflict of interest

Authors declare that they have no conflict of interest.

### ORCID iDs

David Sanchez-Manzano  <https://orcid.org/0000-0003-1229-6868>

M Garcia-Hernandez  <https://orcid.org/0000-0002-5987-0647>

C Feuillet-Palma  <https://orcid.org/0000-0002-8389-5756>

J Lesueur  <https://orcid.org/0000-0002-5843-187X>

C Leon  <https://orcid.org/0000-0002-3262-1843>

J Santamaria  <https://orcid.org/0000-0003-4594-2686>

### References

- [1] Bergeret F S, Volkov A F and Efetov K B 2001 Long-range proximity effects in superconductor-ferromagnet structures *Phys. Rev. Lett.* **86** 4096–9
- [2] Eschrig M, Kopp J, Cuevas J C and Schön G 2003 Theory of half-metal/superconductor heterostructures *Phys. Rev. Lett.* **90** 4
- [3] Buzdin A I 2005 Proximity effects in superconductor-ferromagnet heterostructures *Rev. Mod. Phys.* **77** 935–76
- [4] Bergeret F S, Volkov A F and Efetov K B 2005 Odd triplet superconductivity and related phenomena in superconductor-ferromagnet structures *Rev. Mod. Phys.* **77** 1321
- [5] Houzet M and Buzdin A 2007 Long range triplet Josephson effect through a ferromagnetic trilayer *Phys. Rev. B* **76** 060504
- [6] Asano Y, Tanaka Y and Golubov A A 2007 Josephson effect due to odd-frequency Pairs in diffusive half metals *Phys. Rev. Lett.* **98** 107002
- [7] Sperstad I B, Linder J and Sudbø A 2008 Josephson current in diffusive multilayer superconductor/ferromagnet/superconductor junctions *Phys. Rev. B* **78** 104509
- [8] Halterman K, Valls O T and Barsic P H 2008 Induced triplet pairing in clean s-wave superconductor/ferromagnet layered structures *Phys. Rev. B* **77** 174511
- [9] Eschrig M and Löfwander T 2008 Triplet supercurrents in clean and disordered half-metallic ferromagnets *Nat. Phys.* **4** 138–43
- [10] Keizer R S, Goennenwein S T B, Klapwijk T M, Miao G, Xiao G and Gupta A 2006 A spin triplet supercurrent through the half-metallic ferromagnet CrO<sub>2</sub> *Nature* **439** 825–7
- [11] Khaire T S, Khasawneh M A, Pratt W P and Birge N O 2010 Observation of spin-triplet superconductivity in co-based Josephson junctions *Phys. Rev. Lett.* **104** 137002
- [12] Anwar M S, Czeschka F, Hesselberth M, Porcu M and Aarts J 2010 Long-range supercurrents through half-metallic ferromagnetic CrO<sub>2</sub> *Phys. Rev. B* **82** 100501
- [13] Robinson A W J, Witt S D J and Blamire M G 2010 Controlled injection of spin-triplet supercurrents into a strong ferromagnet *Science* **329** 59–61
- [14] Klose C et al 2012 Optimization of spin-triplet supercurrent in ferromagnetic Josephson junctions *Phys. Rev. Lett.* **108** 127002
- [15] Glick J A, Aguilar V, Gougam A B, Niedzielski B M, Gingrich E C, Loloee R, Pratt W P and Birge N O 2018 Phase control in a spin-triplet SQUID *Sci. Adv.* **4** eaat9457
- [16] Linder J and Robinson J W A 2015 Superconducting spintronics *Nat. Phys.* **11** 307–15
- [17] Eschrig M 2015 Spin-polarized supercurrents for spintronics: a review of current progress *Rep. Prog. Phys.* **78** 104501
- [18] Sefrioui Z, Arias D, Peña V, Villegas J E, Varela M, Prieto P, León C, Martínez J L and Santamaria J 2003 Ferromagnetic/superconducting proximity effect in La<sub>0.7</sub>Ca<sub>0.3</sub>MnO<sub>3</sub>/YBa<sub>2</sub>Cu<sub>3</sub>O<sub>7-δ</sub> superlattices *Phys. Rev. B* **67** 214511
- [19] Dybko K, Werner-Malento K, Aleshkevych P, Wojcik M, Sawicki M and Przysluski P 2009 Possible spin-triplet superconducting phase in the La<sub>0.7</sub>Sr<sub>0.3</sub>MnO<sub>3</sub>/YBa<sub>2</sub>Cu<sub>3</sub>O<sub>7</sub>/La<sub>0.7</sub>Sr<sub>0.3</sub>MnO<sub>3</sub> trilayer *Phys. Rev. B* **80** 144504
- [20] Visani C, Sefrioui Z, Tornos J, Leon C, Briatico J, Bibes M, Barthélémy A, Santamaría J and Villegas J E 2012 Equal-spin Andreev reflection and long-range coherent transport in high-temperature superconductor/half-metallic ferromagnet junctions *Nat. Phys.* **8** 539–43
- [21] Kalcheim Y, Millo O, Egilmez M, Robinson J W A and Blamire M G 2012 Evidence for anisotropic triplet superconductor order parameter in half-metallic ferromagnetic La<sub>0.7</sub>Ca<sub>0.3</sub>Mn<sub>3</sub>O proximity coupled to superconducting Pr<sub>1.85</sub>Ce<sub>0.15</sub>CuO<sub>4</sub> *Phys. Rev. B* **85** 104504
- [22] Egilmez M, Robinson J W A, MacManus-Driscoll J L, Chen L, Wang H and Blamire M G 2014 Supercurrents in half-metallic ferromagnetic La<sub>0.7</sub>Ca<sub>0.3</sub>MnO<sub>3</sub> *Europhys. Lett.* **106** 37003
- [23] Visani C, Cuellar F, Pérez-Muñoz A, Sefrioui Z, León C, Santamaría J and Villegas J E 2015 Magnetic field influence on the proximity effect at YBa<sub>2</sub>Cu<sub>3</sub>O<sub>7</sub>/La<sub>2/3</sub>Ca<sub>1/3</sub>MnO<sub>3</sub> superconductor/half-metal interfaces *Phys. Rev. B* **92** 014519
- [24] Sanchez Manzano D et al 2022 Extremely long-range, high-temperature Josephson coupling across a half-metallic ferromagnet *Nat. Mater.* **21** 188
- [25] de Gennes P G 1964 *Rev. Mod. Phys.* **36** 225
- [26] Müller G M et al 2009 *Nat. Mater.* **2008** 56
- [27] Likharev K K 1976 *Sov. Tech. Phys. Lett.* **2** 12
- [28] Likharev K K 1979 Superconducting weak links *Rev. Mod. Phys.* **51** 101
- [29] Usadel K D 1970 *Phys. Rev. Lett.* **25** 507



- [30] Dubos P, Courtois H, Pannetier B, Wilhelm F K, Zaikin A D and Schön G 2001 Josephson critical current in a long mesoscopic S-N-S junction *Phys. Rev. B* **63** 064502
- [31] Courtois H, Ph. Gandit D M and Pannetier B 1996 *Phys. Rev. Lett.* **76** 130
- [32] Kabasawa U, Tanitani Y, Fukazawa T, Tsukamoto A, Masahiko Hiratani M H and Kazumasa Takagi K T 1991 *Jpn. J. Appl. Phys.* **1** 1670
- [33] Kozono Y, Kasai M and Kanke Y Ohno T, Hanazono M, and Sugita Y 1991 *Physica C* **185–189** 1919
- [34] Boguslavskii Y M and Gao J 1992 *Physica C* **194** 268
- [35] Satoh T, Hidaka M, Yu K M, Hidaka M and Tsuge H 1995 *IEEE Trans. Appl. Supercond.* **5** 2612
- [36] Kupriyanov M Y and Tsai J S 1995 *IEEE Trans. Appl. Supercond.* **5** 2531
- [37] Devyatov I A and Kupriyanov M Y 1997 *JETP* **85** 189
- [38] Hoffmann A, te Velthuis S G E, Sefrioui Z, Santamaría J, Fitzsimmons M R, Park S and Varela M 2005 Suppressed magnetization in  $\text{La}_{0.7}\text{Ca}_{0.3}\text{MnO}_3$   $\text{YBa}_2\text{Cu}_3\text{O}_{7-\delta}$  superlattices *Phys. Rev. B* **72** 140407
- [39] Salafranca J and Okamoto S 2010 Unconventional proximity effect and inverse spin-switch behavior in a model manganite-cuprate-manganite trilayer system *Phys. Rev. Lett.* **105** 256804
- [40] Visani C *et al* 2011 *Phys. Rev. B* **84** 060405(R)
- [41] Bhatia E, Srivastava A, Devine-Stoneman J, Stelmashenko N A, Barber Z H, Robinson J W A and Senapati K 2021 Nanoscale domain wall engineered spin-triplet Josephson junctions and SQUID *Nano Lett.* **21** 3092–7
- [42] Ivachenko Y M and Zil'berman L A 1969 The Josephson effect in small tunnel contacts *Sov. J. Exp. Theor. Phys.* **28** 1272
- [43] Koch R H, Foglietti V, Gallagher W J, Koren G, Gupta A and Fisher M P A 1989 Experimental evidence for vortex-glass superconductivity in Y-Ba-Cu-O *Phys. Rev. Lett.* **63** 1511
- [44] Anwar M S, Veldhorst M, Brinkman A and Aarts J 2012 Long range supercurrents in ferromagnetic  $\text{CrO}_2$  using a multilayer contact structure *Appl. Phys. Lett.* **100** 052602
- [45] Tanaka Y and Golubov A A 2007 Theory of the proximity effect in junctions with unconventional superconductors *Phys. Rev. Lett.* **98** 037003
- [46] Tusei C C and Kirtley J R 2000 *Rev. Mod. Phys.* **72** 969
- [47] Volkov A F and Efetov B K 2009 Proximity effect and its enhancement by ferromagnetism in high-temperature superconductor-ferromagnet structures *Phys. Rev. Lett.* **102** 077002
- [48] Laughlin R B 1998 Magnetic induction of  $\text{dx}^2-\text{y}^2+\text{id}_{xy}$  order in high-  $T_c$  superconductors *Phys. Rev. Lett.* **80** 5188
- [49] Franz M and Tesanovic Z 1998 Self-consistent electronic structure of a  $\text{dx}^2-\text{y}^2$  and a  $\text{dx}^2-\text{y}^2+\text{id}_{xy}$  Vortex *Phys. Rev. Lett.* **80** 4763
- [50] Balatsky A V 2000 Field-induced  $\text{d}_{x^2-y^2}^2+\text{id}_{xy}$  state and marginal stability of high- $T_c$  superconductors *Phys. Rev. Lett.* **61** 6940